



Surface chemical analysis of spatter particles generated in laser powder bed fusion of Hastelloy X in process atmospheres with high and low oxygen

Downloaded from: <https://research.chalmers.se>, 2025-12-04 22:41 UTC




Citation for the original published paper (version of record):

de Andrade Schwerz, C., Cao, Y., Nyborg, L. (2023). Surface chemical analysis of spatter particles generated in laser powder bed fusion of Hastelloy X in process atmospheres with high and low oxygen content. *Surface and Interface Analysis*, 55(6-7): 396-403. <http://dx.doi.org/10.1002/sia.7202>

N.B. When citing this work, cite the original published paper.

RESEARCH ARTICLE

Surface chemical analysis of spatter particles generated in laser powder bed fusion of Hastelloy X in process atmospheres with high and low oxygen content

Claudia Schwerz  | Yu Cao  | Lars Nyborg 

Department of Industrial and Materials
Science, Chalmers University of Technology,
Gothenburg, Sweden

Correspondence

Claudia Schwerz, Department of Industrial and
Materials Science, Chalmers University of
Technology, SE 412 96 Gothenburg, Sweden.
Email: claudia.schwerz@chalmers.se

Funding information

European Union's Horizon 2020, Grant/Award
Number: 820774

Additive manufacturing, particularly laser powder bed fusion (LPBF), has received much attention in recent years because of its multiple benefits over traditional manufacturing. One of the key factors affecting the repeatability and performance of the materials is the existence of defects. Defects can be driven by process by-products called spatters, which consist of particles covered by an oxide layer formed during their travel time in the process atmosphere. As a standard process atmosphere consists of argon containing a residual oxygen level of around 0.1%, one possible way of addressing spatter-driven defect formation is by reducing the oxygen level, thereby reducing the oxidation of the spatter particles. In this study, Hastelloy X powder was processed by means of LPBF in an argon atmosphere containing 1000-ppm O₂ or 50-ppm O₂. Spatter particles were collected in a controlled manner, allowing sampling particles of different sizes, which were analyzed in terms of their surface chemical composition by means of X-ray photoelectron spectroscopy (XPS) and Auger electron spectroscopy (AES). By combining these two tools, a comprehensive assessment of the surface chemical composition was conducted, taking advantage of XPS for the evaluation of the overall surface chemistry and of Auger nanoprobe analysis for high lateral analytical resolution combined with depth profiling. It is shown that tighter oxygen control will both limit the overall oxidation and affect the surface chemical composition. At regular O₂ level in the process atmosphere (1000 ppm), spatter particles are covered by a 70-nm-thick oxide layer, on average. The thickness is substantially greater than that measured in spatter particles collected from the process atmosphere containing 50-ppm oxygen, which averages 6 nm and is comparable with that of the virgin powder, thus revealing a potential for defect mitigation through control of the process atmosphere. Nonetheless, substantial differences in the surface chemical composition were identified between spatters and virgin powder, notably with the appearance of Al- and Ti-oxides on spatter particles, revealing the influence of the manufacturing process on surface characteristics.

This is an open access article under the terms of the [Creative Commons Attribution-NonCommercial](https://creativecommons.org/licenses/by-nc/4.0/) License, which permits use, distribution and reproduction in any medium, provided the original work is properly cited and is not used for commercial purposes.

© 2023 The Authors. *Surface and Interface Analysis* published by John Wiley & Sons Ltd.

KEYWORDS

additive manufacturing, AES, oxidation, spatter, XPS

1 | INTRODUCTION

One growing field of use of metal powder is powder bed-based additive manufacturing. In such processes, the interest in producing fine surfaces and fine details has pushed for the use of fine powder. For laser powder bed fusion (LPBF), the particle size distribution (PSD) is typically between 15 and 45 μm . These particles interact with a laser beam during the manufacturing process, typically in an argon atmosphere containing under 1000-ppm oxygen, a standard limit used by the main LPBF machine manufacturers. Because of the high surface-to-volume ratio combined with interaction with a laser beam in an atmosphere containing oxygen, surface characteristics become important.

During manufacturing, process by-products known as spatter are formed. These particles consist of melt pool ejecta,^{1,2} particles entrained in the low-pressure zone created by the vapor jet,^{3,4} or scattered particles¹ that can interact with the laser beam, the process atmosphere, and with one another, generating different subtypes of spatter. Spatter particles can be substantially larger than the feedstock powder,⁵ over 200 μm , and are typically oxidized.⁶ Because of these characteristics, when redeposited on the powder bed, spatter particles can trigger defects, as the laser beam is hindered from effectively melting these particles and incorporating them into the material.^{7,8} Defects known as lack of fusion are formed in such cases and have been observed to occur preferentially in the direction of gas flow in the chamber⁷⁻⁹ as a result of the travel of these particles and their incomplete removal from the process envelope.

The exact defect formation mechanism associated with spatters is still debatable. Esmaeilzadeh et al.⁸ attributed defect formation to the local increase of the thickness of the powder layer resulting from spatter deposition, whereas Ladewig et al.⁷ attributed it to the laser beam attenuation promoted by the spatter particles, both of which hinder complete melting. Other authors have attributed spatter-induced defect formation to chemical contamination¹⁰ or, more specifically, the surface oxide layers¹¹ present in spatter particles as a result of their selective oxidation in-process. Hence, two main characteristics of spatter particles, their increased size in relation to the feedstock powder and their oxidized surface, likely contribute to defect formation. It is crucial to determine the contribution of each of these factors to develop suitable defect mitigation strategies. This study investigates the oxidized surface of spatter particles. In case the spatter surface state governs defect formation, then one potential defect mitigation strategy is to further restrict the oxygen content in the process atmosphere to limit the oxygen pickup of the particles, thus favoring the incorporation of spatter particles into the bulk material and preventing defect formation. In this study, this strategy is investigated for the Ni-base alloy Hastelloy X. The approach consists of comparing spatter collected from two builds performed in an argon

atmosphere, one containing a maximum of 1000-ppm oxygen and one restricted to 50-ppm oxygen. Spatter particles were collected in two distinct locations in the build chamber, in which the mixing with the feedstock powder is deemed minimal. These particles were characterized in terms of surface morphology and chemistry through the combination of XPS and AES, which enable the evaluation of the surface chemistry, and high lateral analytical resolution combined with depth profiling, respectively.

2 | MATERIALS AND METHODS

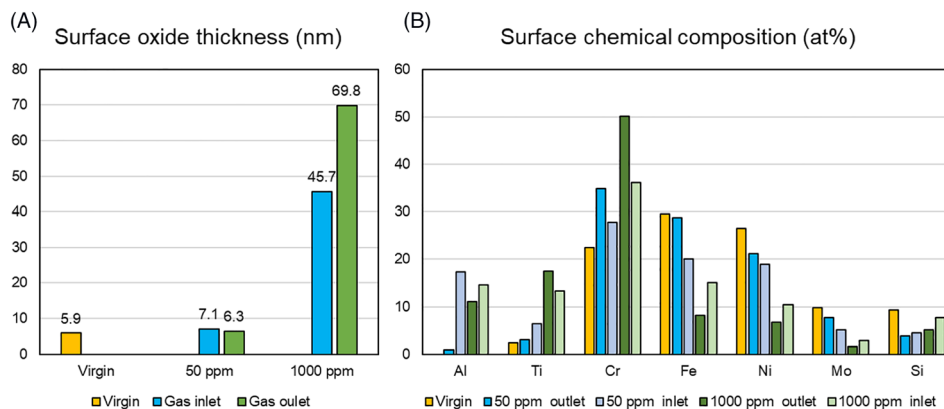
The feedstock material used is gas-atomized Hastelloy X with particle size d10 of 18.7 μm , d90 of 57.6 μm , and d50 of 34.8 μm . The nominal chemical composition corresponds to UNS N06002 and is indicated in Table 1.

The feedstock powder was processed in an LPBF M290 machine (EOS GmbH) in an argon atmosphere with two different oxygen contents. The builds are identical, both in terms of geometry and parameters used, factors known to affect spatter formation and redeposition.^{1,5,9,12} Prior to the build processes, the chamber was flooded with argon. In one of the builds, the process was initiated once the oxygen concentration in the atmosphere was stabilized at less than 1000 ppm, which is the default in this additive manufacturing system. In the second build, the ADDvance O₂ precision system (Linde plc) was employed in combination with the LPBF machine to further limit the oxygen content in the atmosphere to a maximum of 50 ppm. Each build process lasted about 22 h and was done according to optimized practice to yield >99.9% relative density.¹³ During the process, by-products (spatters) were formed, traveled, and accumulated in different locations within the build chamber. After the building processes were completed, spatter particles were sampled from the gas inlet and from the gas outlet.

The spatter samples were characterized in terms of surface chemistry via XPS and AES. Sample preparation was performed by pressing the particles onto copper plates (for XPS) and aluminum plates (for AES). The XPS was conducted by means of a PHI 5500 VersaProbe III scanning XPS microprobe (ULVAC-PHI) equipped with monochromatic aluminum K α X-ray source (1486.6 eV) with a beam size of 200 or 50 μm . In the latter case, an X-ray-induced second electron image was used for navigation of individual particles. Quantification of XPS results in terms of apparent surface composition was done by means of XPS peak intensities using sensitivity factors provided by PHI. The AES analyses were conducted with a PHI 700 scanning Auger nanoprobe (ULVAC-PHI). The electron accelerating voltage was 10 kV, and the beam current was 10 nA, enabling a nominal analytical lateral resolution of ~ 20 nm. Images were registered frequently to ensure that the data were acquired at the intended location.

TABLE 1 Nominal composition of the feedstock powder. The minimum and maximum weight percentages of each element are presented.

	Ni	Cr	Fe	Mo	W	Co	C	Si	Mn	S	P	B	Se	Cu	Al	Ti
Min.	Bal.	20.5	17.0	8.0	0.2	0.5	--	--	--	--	--	--	--	--	--	--
Max.		23.0	20.0	10.0	1.0	2.5	0.1	1.0	1.0	0.03	0.04	0.01	0.005	0.5	0.5	0.15

FIGURE 1 XPS measurements performed on the virgin powder and spatter particles. (A) Surface oxide thickness; (B) surface chemical composition (not accounting for oxygen and carbon).

Compositional depth profiling was performed via successive XPS/AES analyses and Ar^+ ion etching over an area of 2×2 mm with an ion beam accelerating voltage of 2.0 kV. The nominal angle of ion incidence with respect to the sample surface was 33° for XPS and 48° for AES. The nominal etch rate was calibrated by using flat $\text{Ta}_2\text{O}_5/\text{Ta}$ samples and corresponded to 5.1 nm/min for both instruments. $\text{Ta}_2\text{O}_5/\text{Ta}$ with well-known oxide thickness is a commonly used reference for etch rate calibration when performing depth profiling using XPS and AES¹⁴ and is expected to be of the same order of magnitude as the oxides on the analyzed powder.¹⁵ The oxide thickness was defined as the depth where the intensity of oxygen decreases by half.

3 | RESULTS AND DISCUSSION

3.1 | Overall surface chemistry

XPS was used to measure the overall oxidation state and surface oxide thickness on virgin powder and spatter particles collected from the different builds. As the measurement area is relatively large, the analyses include tens of particles, thus providing average values of the quantities measured. With this, the overall changes in surface chemistry from the virgin powder to the spatter particles collected from different processing atmospheres and sampling locations can be observed.

3.1.1 | Thickness of the surface oxide layer

The surface oxide layer thickness was measured using an X-ray beam size of 200 μm on spatter particles collected by the gas inlet and gas

outlet for standard processing atmosphere (1000 ppm) and with tighter oxygen control (50 ppm). Corresponding measurements were performed in the virgin powder as a reference. The oxide thickness is estimated when the oxygen intensity is decreased by half, according to the method developed by Nyborg et al.¹⁶ The results, summarized in Figure 1A, reveal a negligible increase in the oxide thickness compared with the virgin state when the oxygen content is kept under 50 ppm in the process atmosphere. Additionally, no significant difference is identified in the oxide thickness at different sampling locations for the 50-ppm oxygen atmosphere. However, the oxide thicknesses measured for spatters collected in the build with 1000-ppm oxygen were location-dependent, with an average of about 70 nm for the particles collected at the gas outlet and about 46 nm for the gas inlet.

The thickness of the surface oxide layer was also measured by means of XPS depth profiling for some individual particles of dimensions larger than the feedstock powder, collected on the gas inlet in the 1000-ppm oxygen build. A 50- μm beam diameter was used for these analyses. The first particle, spherical with an approximate diameter of 145 μm , was covered with a 47.9-nm-thick oxide layer, and the second particle, an agglomerate of two particles with a maximum length of about 70 μm , had a surface oxide layer thickness of 43.4 nm. Thus, the surface oxide thicknesses measured for individual particles appear to fit with the average oxide thickness measured across a larger area (estimated to be $\sim 400 \times 400 \mu\text{m}^2$) of a sample collected in the same conditions, where the average surface oxide thickness is 45.7 nm. Even with reduced X-ray beam size and consequently smaller analysis area, it is not possible to determine via XPS whether there are any inhomogeneities in the oxidation of the spatter particles sampled. For that, complementary analyses are required and will be presented in the next section.

3.1.2 | Surface chemical composition

The apparent surface chemical composition was measured by means of XPS. The results are summarized in Figure 1B, in which the apparent relative atomic concentrations of the metallic elements in their oxide state on the sample surfaces are presented. The data refer to the analysis of the Al2p, Ti2p^{3/2}, Cr2p^{3/2}, Fe^{1/2} (instead of Fe_{3/2} to minimize interference with Ni LMM), Ni2p^{3/2}, Mo3d^{5/2}, and Si2s. Note that C and O were not included in the quantification. Even though a similar surface oxide thickness was measured for the virgin powder and the spatter samples when the oxygen content in the atmosphere was below 50 ppm, their surface chemical compositions differ substantially, indicating the influence of the manufacturing process on the surface oxide characteristics. The elements Cr, Ni, Fe, Si, Mo, and a small amount of Ti are found on the surface of the virgin powder. On the spatter particles, Al is additionally identified and Si is lost. These results are consistent with those of Shvab et al.¹⁷ on the surface chemical characterization of virgin and reused Hastelloy X powder, where the segregation and surface oxidation of strong oxide-forming elements (Al and Cr) were observed, and the loss of Si on the surface due to sublimation was indicated for the reused powder. In the present study, the surface contents of Cr and Ti are consistently and substantially higher for the spatter particles collected for the 1000-ppm oxygen than those collected in the 50-ppm condition, which leads to proportional decreases in the content of Ni, Fe, and Mo. Carbon has been identified on the surface of all samples, but as

its content decreases rapidly with etching, its presence is attributed to contamination¹⁷ and not considered relevant.

3.2 | Auger electron spectroscopy

Albeit possible, the evaluation of the surface oxidation of individual particles via XPS is experimentally challenging. A more suitable technique to further explore the surface chemistry of spatter particles is AES. Thanks to the high lateral resolution of the technique, it is possible to assess the local inhomogeneity of both oxide thickness and composition on the particle surfaces.

3.2.1 | Point depth profiling and point analysis

AES was used for depth profiling of spatter particles collected in both conditions, 50- and 1000-ppm oxygen in the process atmosphere. The morphology and chemical composition of the surface oxides is not expected to vary remarkably and consistently with the sampling location, as observed in Figure 1; therefore, the AES analysis is limited to the particles collected by the gas outlet, where substantially thicker oxides were identified for the 1000-ppm case. For each sample, 20 particles of varying sizes and morphologies were selected for analysis, as indicated in Figure 2. The different coverages of particles in the images are merely a result of the sample preparation. A tighter

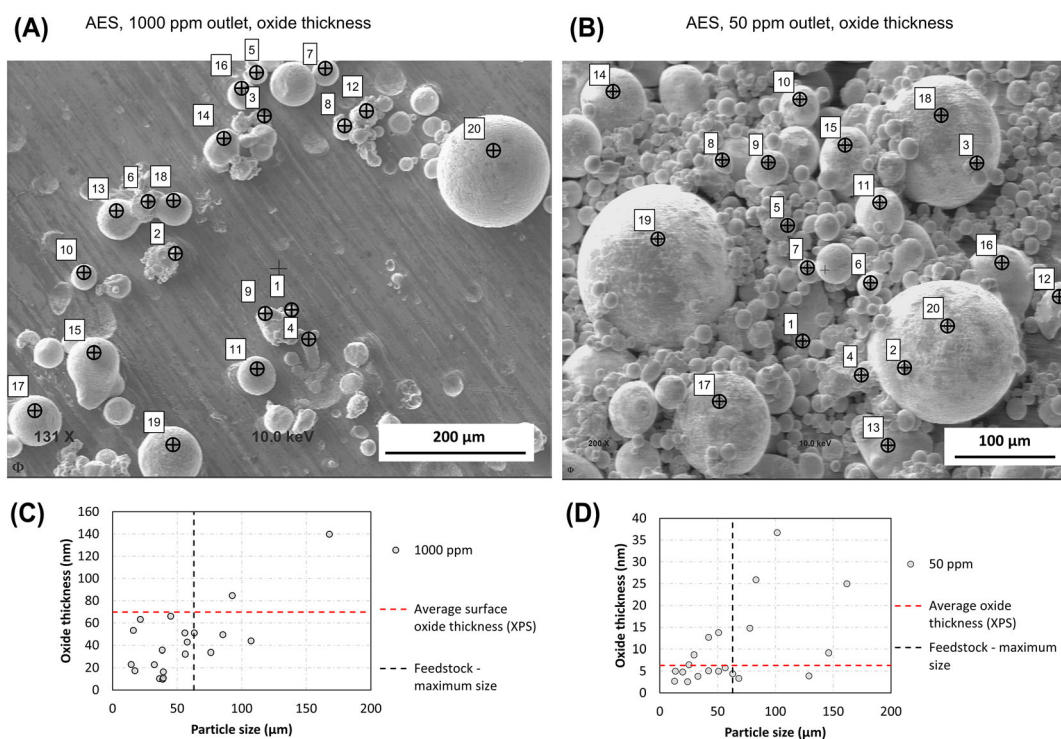


FIGURE 2 Oxide thickness measured in 20 different particles of (A) 1000-ppm gas outlet sample and (B) 50-ppm gas outlet sample. The measurement locations are indicated by a cross and are labeled 1 to 20. (C) and (D) show the oxide thickness plotted against the particle size for the 1000- and 50-ppm samples, respectively.

packing of particles on the substrate allowed for the sampling of a larger number of large particles. The position for depth profiling was selected consistently on all particles to keep the angle of ion incidence as similar as possible in order to keep a consistent etch rate.¹⁸ For the measurement strategy in question, it can be envisaged that differences in oxide thickness can be depicted when significant. For the 1000-ppm sample, the surface oxide thickness varies from about 10 to 140 nm, whereas for the 50-ppm sample, the thickness determined was from less than 3 nm to around 40 nm. In both cases, the average oxide thickness measured via XPS is within these ranges (about 70 and 6 nm, respectively), showing consistency between the measurement techniques but significant particle-to-particle variation. In both cases, the highest oxide thickness was measured in particles necessarily generated in-process, that is, in particles larger than 63 μm , which corresponds to the sieve opening and is, therefore, the maximum feedstock particle size. Interestingly, in the case of 1000-ppm spatter, only two oxide thickness measurements were above the average value measured via XPS, which indicates an over-representation of these particles.

The depth profiles revealed that the relative amounts of preferentially oxidized elements on particle surfaces differ among particles. Figure 3 illustrates this variation by representing the depth profiles from the locations in which the thickest oxides were measured. For spatter sampled from the process atmosphere containing up to 1000-ppm oxygen, the thickest oxide measured (Figure 3A) contained mainly Cr, Ti, and Al, in this order, and the second thickest oxide

(Figure 3B) contained mainly Al, and Ti to a lesser extent. In general, the particles presented Cr-, Al-, and Ti-rich oxides on the surface, as in point 16 in Figure 3C, but predominantly Cr- and Fe-rich surface oxides were also identified. For the spatter sampled from the process atmosphere containing up to 50-ppm oxygen, the surface oxides were mainly rich in Al, as observed in Figure 3D–F. Clearly, across the surfaces of the spatter particles, the oxide is heterogeneous from a chemical point of view. As shown by other authors¹⁹ and below, the oxide composition is associated with different morphological characteristics.

The high-resolution images shown in Figure 4 reveal the various morphological features on the surface of 1000-ppm spatter particles, the most prevalent being vermicular (points 1 and 2), dot (points 3 and 4), scale (points 5 and 6), and web (points 7 and 8). Additionally, featureless regions are present (points 9 and 10). To further investigate the surface chemistry, high-resolution AES was performed on these morphological features on several particles. It was found that dot features are rich in Al mainly but also contain significant quantities of Ti and Cr; scale features are rich in Al, with smaller amounts of Ti, Cr, and Si. Vermicular features contain mainly Cr, with the second most prevalent element varying from region to region, but most commonly Ti or Si. Web features are rich in Cr, Ti, and Si. The featureless regions also consist of oxides, rich in Cr, Ti, and Al in varying ratios.

Characteristic examples of AES analyses are shown in Figures 5 and 6 for spatter particles sampled by the gas outlet at 1000-ppm O_2 and 50-ppm O_2 conditions, respectively. It is assumed that all metallic

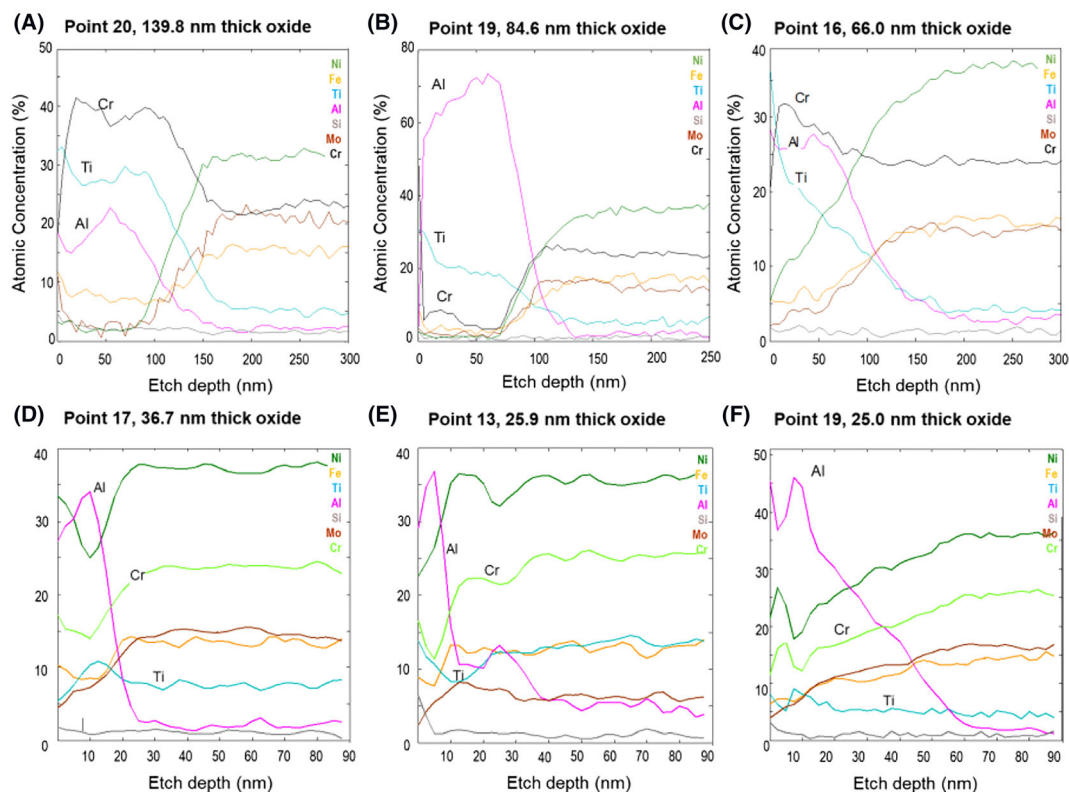


FIGURE 3 Depth profiles measured in distinct spatter particles collected on the gas outlet from the build containing 1000-ppm (A–C) and 50-ppm (D–F) oxygen in the atmosphere. The point IDs correspond to those in Figure 1.

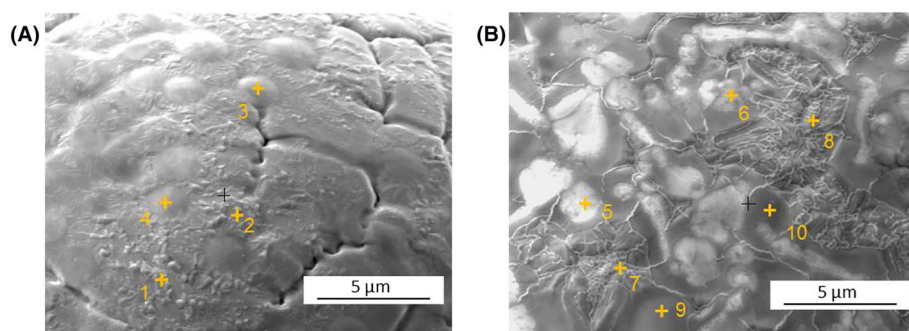


FIGURE 4 Surface of spatter particles sampled from the process containing up to 1000-ppm oxygen in the atmosphere. Oxides are present in diverse morphologies, the most prevalent being vermicular (points 1 and 2), dot (3 and 4), scale (5 and 6), and web (7 and 8). Some regions are apparently featureless, as on points 9 and 10.

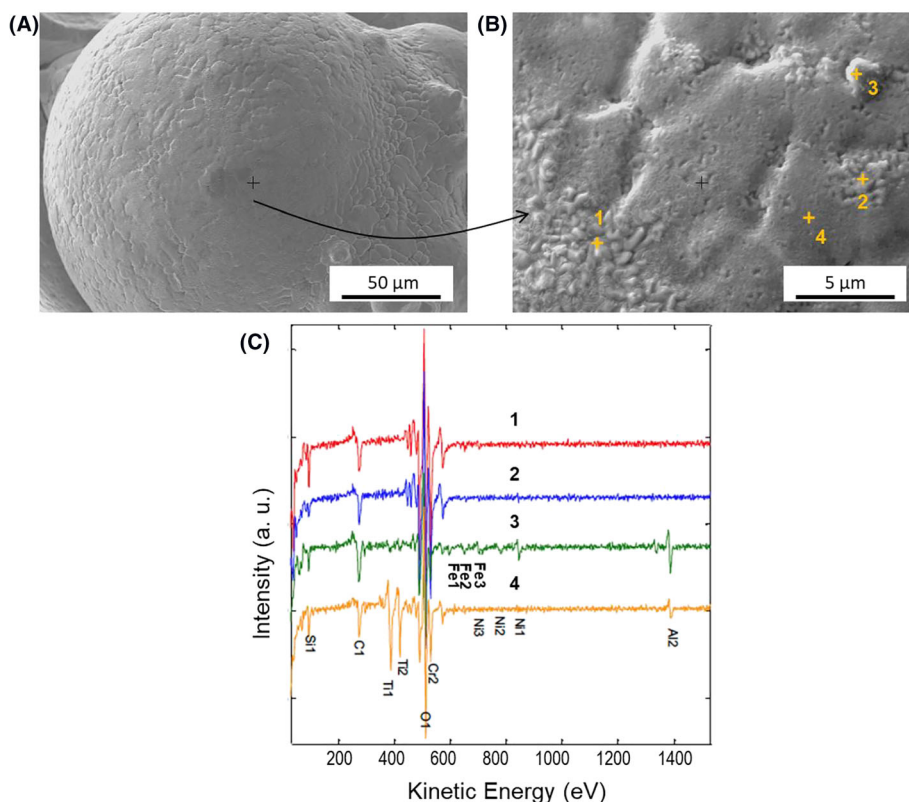
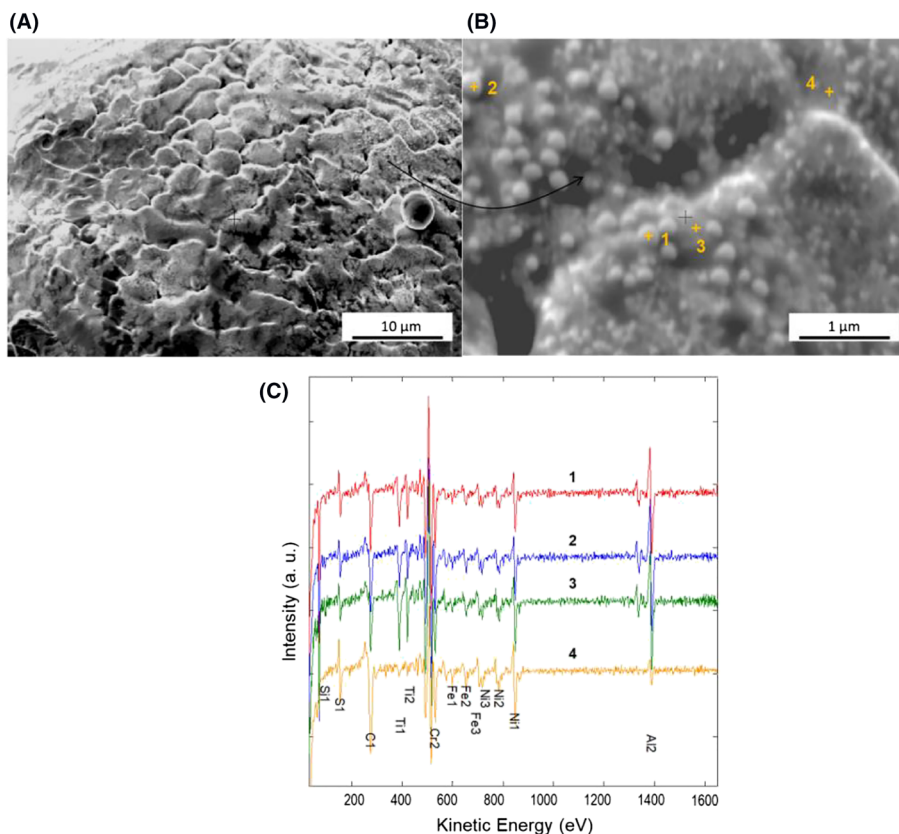


FIGURE 5 Selected spatter particle sampled from the process containing up to 1000-ppm oxygen in the atmosphere at low (A) and high magnification (B) with high lateral resolution AES spectra (C) recorded from indicated locations in (B).

elements are present in their oxide states. The features in locations 1 and 2 in Figure 5 have a vermicular morphology and can be viewed as Cr-rich oxide with potential Si contamination on top, and the feature in location 3 (particulate morphology) shows evidence of a strong presence of Al, Cr, and Ni. Then, the analysis in location 4 (morphologically featureless) shows a strong presence of Ti and Cr in combination, with evidence of Al and potentially Si. In all these cases, Si is identifiable by the low kinetic energy peak, which indicates that Si can only be present on the outermost surface. It is suggested that the presence of Si is a result of an evaporation and condensation mechanism, following the observations by Shvab et al.²⁰ The surface enrichment and oxidation of strong oxide formers such as Al, Ti, and Cr can be expected from the fact that the spatter particle would experience high temperatures, most probably molten state. This would allow diffusion to the surface of spatter particles, despite their transient rapid heating and cooling.

The heterogeneous oxide formation is also evident for gas outlet spatter particles from the 50-ppm O₂ atmosphere. Figure 6 shows a close-up view of such spatter particle presenting surface oxide with scale morphology and the corresponding AES analyses in selected locations on the surface. Besides O, locations 1–3 show high Al, the predominant expected oxide-forming element for the observed morphology, Ti, Cr, and Ni, as well as some Fe. In location 4, Ti is not evident, and Al is present in smaller amounts. Locations 1–3 are selected to depict the surface chemistry of the features, and it is supposed that there is selective oxidation of Al, Ti, and Cr. Therefore, a lower oxygen availability does not eliminate spatter oxidation. The total oxidation level is decreased, but, in fact, selective oxidation can be even more severe. This can be expected from the following argument: As long as the availability of any strong oxide former can balance the oxygen from the process atmosphere, for example, when the particle is molten or just being solidified, the thermodynamics and kinetics promote

FIGURE 6 Close-up view (A and B) of gas outlet spatter particle for the 50-ppm O₂ atmosphere condition. Selected point AES analyses (C) on locations indicated in (B).



selective oxidation, as is also observed. Furthermore, compared with gas-atomized powder experiencing exposure to atomizing gas with a finite amount of oxygen, the surface oxide formed then is heterogeneous in chemistry and morphology. The same is observed here for the spatter particle analysis and hence consistent with what could be expected for particles undergoing rapid solidification and cooling in an oxygen-containing atmosphere.

4 | CONCLUSIONS

In this study, a comprehensive assessment of the surface chemical composition of spatter particles was conducted, taking advantage of XPS for the evaluation of the overall surface chemical composition and oxide thickness and of Auger nanoprobe analysis for high lateral analytical resolution combined with depth profiling. It was found that the average surface oxide thickness of spatters collected from the process with standard oxygen level (1000 ppm) is significantly higher than that measured from 50-ppm oxygen, with an 11-fold difference for the particles collected on the gas outlet and 6.5-fold for the gas inlet. In the 1000-ppm oxygen atmosphere, the average surface oxide thickness of spatters collected from the gas outlet is 50% higher than that from the gas inlet. This result suggests that the pronounced defect formation previously observed in parts built adjacent to the gas outlet⁹ can be a result of the combined larger quantity of spatter landing in this location and the larger extent of their oxidation. Point-based depth profiles in individual particles revealed an important

particle-to-particle variation in terms of surface oxide thickness. For spatters collected from the 1000-ppm oxygen atmosphere, the measurements varied from 9.7 to 139.8 nm and from 2.6 to 36.7 nm for the 50-ppm oxygen spatters. This variability can be yet another reason why some spatter particles are fully incorporated into the bulk and others are not, thus generating defects.

The restriction of oxygen content in the process atmosphere to 50 ppm renders the surface oxide thickness of spatter particles comparable with those of the feedstock powder in both sampling locations, gas outlet and inlet. This result is promising in case the extent of oxidation of spatter particles is, in fact, a decisive factor driving the formation of defects. However, the surface chemical compositions of these spatter samples and virgin powder differ substantially, marking the influence of the manufacturing process on the surface characteristics and potentially impacting their behavior in-process. The spatter particles sampled from this condition presented surface oxides predominantly with scale morphology, rich mainly in Al, indicating more severe selective oxidation than the process atmosphere richer in oxygen. It is important to highlight that the lower oxygen content in the process atmosphere does not prevent large spatter particles from forming, and these particles tend to be covered by a thicker oxide layer, albeit thinner than the average for the 1000-ppm oxygen condition.

On top of particle-to-particle variations, inhomogeneities on the surface of single particles were consistently observed. These inhomogeneities consist of oxides of different morphologies and chemical compositions, factors that are correlated. Considering the findings in

this study, future work should investigate whether the tight control of oxygen content in the process atmosphere prevents the formation of defects and secures superior, repeatable properties. Furthermore, the surface characteristics of spatter particles observed in the adjacencies of defects should be investigated for a better understanding of their relevance to the formation of defects.

ACKNOWLEDGMENTS

This work was conducted within the framework of the project MANUELA-Additive Manufacturing using Metal Pilot Line, funded by European Union's Horizon 2020 research and innovation program under grant agreement no. 820774 and the Competence Centre for Additive Manufacturing-Metal (CAM2), as well as the Production Area of Advance at Chalmers and LIGHTer Academy. The authors thank RISE Research Institutes of Sweden for lending the ADDvance O2 system.

DATA AVAILABILITY STATEMENT

The data that support the findings of this study are available from the corresponding author upon reasonable request.

ORCID

Claudia Schwerz  <https://orcid.org/0000-0002-3287-7558>

Yu Cao  <https://orcid.org/0000-0002-1965-5854>

Lars Nyborg  <https://orcid.org/0000-0002-1726-5529>

REFERENCES

- Liu Y, Yang Y, Mai S, Wang D, Song C. Investigation into spatter behavior during selective laser melting of AISI 316L stainless steel powder. *Mater des*. 2015;87:797-806. doi:10.1016/j.matdes.2015.08.086
- Khairallah SA, Anderson AT, Rubenchik A, King WE. Laser powder-bed fusion additive manufacturing: physics of complex melt flow and formation mechanisms of pores, spatter, and denudation zones. *Acta Mater*. 2016;108:36-45. doi:10.1016/j.actamat.2016.02.014
- Ly S, Rubenchik AM, Khairallah SA, Guss G, Matthews MJ. Metal vapor micro-jet controls material redistribution in laser powder bed fusion additive manufacturing. *Sci Rep*. 2017;7(1):1-12. doi:10.1038/s41598-017-04237-z
- Bidare P, Bitharas I, Ward RM, Attallah MM, Moore AJ. Fluid and particle dynamics in laser powder bed fusion. *Acta Mater*. 2018;142:107-120. doi:10.1016/j.actamat.2017.09.051
- Wang D, Wu S, Fu F, et al. Mechanisms and characteristics of spatter generation in SLM processing and its effect on the properties. *Mater des*. 2017;117:121-130. doi:10.1016/j.matdes.2016.12.060
- Simonelli M, Tuck C, Aboulkhair NT, et al. A study on the laser spatter and the oxidation reactions during selective laser melting of 316L stainless steel, Al-Si10-Mg, and Ti-6Al-4V. *Metall Mater Trans a Phys Metall Mater Sci*. 2015;46(9):3842-3851. doi:10.1007/s11661-015-2882-8
- Ladewig A, Schlick G, Fisser M, Schulze V, Glatzel U. Influence of the shielding gas flow on the removal of process by-products in the selective laser melting process. *Addit Manuf*. 2016;10:1-9. doi:10.1016/j.addma.2016.01.004
- Esmailizadeh R, Ali U, Keshavarzkermani A, Mahmoodkhani Y, Marzbanrad E, Toyserkani E. On the effect of spatter particles distribution on the quality of Hastelloy X parts made by laser powder-bed fusion additive manufacturing. *J Manuf Process*. 2019;37:11-20. doi:10.1016/j.jmapro.2018.11.012
- Schwerz C, Raza A, Lei X, Nyborg L, Hryha E, Wirdelius H. In-situ detection of redeposited spatter and its influence on the formation of internal flaws in laser powder bed fusion. *Addit Manuf*. 2021;47:102370. doi:10.1016/J.ADDMA.2021.102370
- Wang D, Ye G, Dou W, et al. Influence of spatter particles contamination on densification behavior and tensile properties of CoCrW manufactured by selective laser melting. *Opt Laser Technol*. 2020;121:105678. doi:10.1016/j.optlastec.2019.105678
- Tang M, Pistorius PC. Oxides, porosity and fatigue performance of AISi10Mg parts produced by selective laser melting. *Int J Fatigue*. 2017;94:192-201. doi:10.1016/j.jfatigue.2016.06.002
- Taheri Andani M, Dehghani R, Karamooz-Ravari MR, Mirzaeifar R, Ni J. A study on the effect of energy input on spatter particles creation during selective laser melting process. *Addit Manuf*. 2018;20:33-43. doi:10.1016/j.addma.2017.12.009
- Schwerz C, Nyborg L. Linking in situ melt pool monitoring to melt pool size distributions and internal flaws in laser powder bed fusion. *Metals*. 2021;11(11):1856. doi:10.3390/MET11111856
- Watts JF, Wolstenholme J. *An introduction to surface analysis by XPS and AES*. John Wiley & Sons Ltd; 2003.
- Baer DR, Engelhard MH, Lea AS. Comparison of the sputter rates of oxide films relative to the sputter rate of ARTICLES YOU MAY BE INTERESTED IN. *J Vac Sci Technol a*. 2010;28(5):1060-1072. doi:10.1116/1.3456123
- Nyborg L, Nylund A, Olefjord I. Thickness determination of oxide layers on spherically-shaped metal powders by ESCA. *Surf Interface Anal*. 1988;12(2):110-114. doi:10.1002/sia.740120209
- Raza A, Pauzon C, Hryha E, Markström A, Forêt P. Spatter oxidation during laser powder bed fusion of alloy 718: dependence on oxygen content in the process atmosphere. *Addit Manuf*. 2021;48:102369. doi:10.1016/J.ADDMA.2021.102369
- Norell M, Nyborg L, Tunberg T, Olefjord I. Thickness determination of surface oxides on metal powder by AES depth profiling. *Surf Interface Anal*. 1992;19(1-12):71-76. doi:10.1002/SIA.740190116
- Gasper AND, Szost B, Wang X, et al. Spatter and oxide formation in laser powder bed fusion of Inconel 718. *Addit Manuf*. 2018;24:446-456. doi:10.1016/j.addma.2018.09.032
- Shvab R, Leicht A, Hryha E, Nyborg L. Characterization of the virgin and recycled nickel alloy hx powder used for selective laser melting, World PM 2016 Congr. Exhib; 2016.

How to cite this article: Schwerz C, Cao Y, Nyborg L. Surface chemical analysis of spatter particles generated in laser powder bed fusion of Hastelloy X in process atmospheres with high and low oxygen content. *Surf Interface Anal*. 2023; 1-8. doi:10.1002/sia.7202